Chinese Journal of Aeronautics, (2022), 35(2): 320–331

Chinese Society of Aeronautics and Astronautics
& Beihang University

Chinese Journal of Aeronautics

cja@buaa.edu.cn
www.sciencedirect.com

Formability enhancement in hot spinning of titanium alloy thin-walled tube via prediction and control of ductile fracture

Pengfei GAO [a,b], **Chao YU** [a], **Mingwang FU** [b], **Lu XING** [a], **Mei ZHAN** [a,*], **Jing GUO** [c]

[a] *State Key Laboratory of Solidification Processing, Shaanxi Key Laboratory of High-Performance Precision Forming Technology and Equipment, School of Materials Science and Engineering, Northwestern Polytechnical University, Xi'an 710072, China*
[b] *Department of Mechanical Engineering, The Hong Kong Polytechnic University, Hung Hom, Kowloon, Hong Kong 999077, China*
[c] *Institute of Chemical Materials, China Academy of Engineering Physics, Mianyang 621900, China*

Received 21 September 2020; revised 19 October 2020; accepted 9 November 2020
Available online 4 March 2021

KEYWORDS

Control of ductile fracture;
Dynamic recrystallization;
Forming limit;
Hot spinning;
Titanium alloy tube

Abstract The damage and fracture in hot spinning of titanium alloy is a very complex process under the combined effects of microstructure evolution and stress state. In this study, their dependences on processing parameters were investigated by an integrated FE model considering microstructure and damage evolution, and revealing the effects of microstructure and stress states on damage evolution. The results show that the inner surface of workpiece with the largest voids volume fraction is the place with the greatest potential of fracture. This is mainly attributed to the superposition effects of positive stress triaxiality and the smallest dynamic recrystallization (DRX) fraction and β phase fraction at the inner surface. The damage degree is decreased gradually with the increase of initial spinning temperature and roller fillet radius. Meanwhile, it is first decreased and then increased with the increases of spinning pass and roller feed rate, which can be explained based on the variations of β phase fraction, DRX fraction, stress state and tensile plastic strain with processing parameters. In addition, the dominant influencing mechanisms were identified and discussed. Finally, the thickness reduction without defect in the hot spinning of TA15 alloy tube is greatly increased by proposing an optimal processing scheme.
© 2021 Chinese Society of Aeronautics and Astronautics and Beihang University. Production and hosting by Elsevier Ltd. This is an open access article under the CC BY-NC-ND license (http://creativecommons.org/licenses/by-nc-nd/4.0/).

* Corresponding author.
E-mail address: zhanmei@nwpu.edu.cn (M. ZHAN).
Peer review under responsibility of Editorial Committee of CJA.

https://doi.org/10.1016/j.cja.2021.01.002
1000-9361 © 2021 Chinese Society of Aeronautics and Astronautics and Beihang University. Production and hosting by Elsevier Ltd. This is an open access article under the CC BY-NC-ND license (http://creativecommons.org/licenses/by-nc-nd/4.0/).

1. Introduction

Titanium alloy thin-walled tube components have been widely used in aerospace industries due to their excellent mechanical properties, such as high strength, light weight and superior creep strength.[1–3] Hot spinning is one of the most preferable methods to form these components for the advantages of simple tooling, low forming force and high material utilization. However, hot spinning of tube components is a complex local loading process under the effects of multi-factors. In this process, the material undergoes severe and inhomogeneous deformation under a complex stress state, which may lead to various forming defects, such as bugle, flaring and ductile fracture, and further deteriorate the forming quality.[4–7] Especially, in order to satisfy the higher light-weight requirement, the thickness of the formed tube component is getting smaller and smaller. However, the larger wall thickness reduction would greatly increase the risk of the occurrence of ductile fracture defect, then limit the maximum wall thickness reduction without fracture, i.e., the forming limit in hot spinning. Therefore, it is crucial to understand the formation mechanisms of the ductile fracture in hot spinning of titanium alloy thin-walled tubes, and further predict, control and avoid of the fracture, in such a way to eventually improve the forming limit and realize the light-weight forming.

So far, the studies on the prediction and control of fracture in tube spinning are mainly focused on cold spinning process. Zhan et al. [8] established the FE models for the power spinning of LF2M aluminum alloy conical part by integrating the Lemaitre and Cockcroft-Latham fracture criteria, respectively. By comparing with the experimental results, it is found that the Lemaitre fracture criterion can make a better prediction of fracture location. By the combination of FE model and modified Lemaitre fracture criterion, Zhan et al. [9] also successfully predicted the fracture defect in the splitting spinning of 5A02-O aluminum alloy "Y" shaped part. On this basis, they determined the forming limit without fracture defect under various forming parameters. Zeng et al. [10] realized the prediction of fracture defect in the power spinning of 5052 aluminum alloy ellipsoidal component through the FE model embedded Johnson-Cook criterion. In addition, they identified the high-risk area for fracture defect and revealed the effect rules of processing parameters on fracture defect, which laid a foundation for controlling the fracture defect. Ma et al. [11] and Xu et al. [12] evaluated the applicability of various fracture criteria, including the models developed by Oh, McClintock, Brozzo, Rice-Tracey, etc. for prediction of fracture defect during spinning of titanium alloy tube parts. In addition, they evaluated the spinnability of TA2 alloy tube at room temperature. As for the prediction of ductile fracture in hot spinning process, some preliminary studies have been conducted. Zhan et al. [13] modified the Oyane fracture criterion via developing the quantitative relationship among the critical fracture value, temperature and strain rate, which makes it applicable to the hot deformation of materials. In addition, they also applied it to predict the fracture defect in hot spinning of TA15 alloy tube.

However, the above fracture prediction models are all phenomenological based without considering the underlying ductile damage mechanism, i.e., microscale void nucleation, growth and coalescence. For the cold spinning process, these models are preferable because the damage mechanism is relatively simple without the evolution of microstructure. In the hot spinning of titanium alloys, however, the material undergoes a complex hot deformation, leading to the complicated microstructure evolutions, including $\alpha \leftrightarrow \beta$ phase transformation, dynamic recrystallization (DRX), grain orientation rotation and so on.[14–16] These microstructure phenomena will significantly influence the damage and fracture behavior. For example, the $\alpha \leftrightarrow \beta$ phase transformation may change the microscale heterogeneous deformation and then influence void nucleation, growth and coalescence. Furthermore, DRX could result in an obvious flow softening, which in turn affects the damage and fracture behavior in hot spinning of titanium alloy.[17,18] Moreover, the complex macroscale stress state in spinning also play a great role in damage evolution and fracture formation.[19] By integrating a modified Gurson-Tvergaard-Needleman model into FE simulation, Dong et al. [20] found that the shearing process greatly affects the damage and fracture mechanism of SUS304 tube. All of these show that the damage and fracture of titanium alloy in hot spinning is a very complex phenomenon simultaneously affected by microstructure evolution and macroscale stress state. Therefore, there is a critical need to consider these effects in avoidance and control of damage and fracture and further improving the formability of titanium alloys in hot spinning process.

In this paper, an integrated FE model considering the microstructure and damage evolution for hot spinning of TA15 alloy tube was introduced, which can simulate the effects of microstructure evolution and stress state on the fracture behavior. On this basis, the characteristics of damage and fracture, and their dependences on processing parameters were analyzed from the aspects of microstructure, stress state and strain. Moreover, the forming limit is improved by optimizing the processing parameters to control fracture defect. The results will provide a basis and guidance for forming process design and tailoring of product quality in hot spinning of titanium alloy tube.

2. Microstructure and damage integrated FE model

As described in Section 1, the FE simulation by using a certain fracture model has been widely used to investigate the fracture behaviour in plastic forming. It can capture detail deformation information, including stress, strain, damage degree, etc., and the low-cost and high-efficiency decision-making in process design and quality assurance. In this work, an integrated FE model considering the microstructure and damage evolution was applied to predict and control the fracture in hot spinning of titanium alloy.

Fig. 1 shows the schematic of the FE model for modelling of backward flow forming under high temperature. The inner diameter and outer diameter of billet are 308 and 346 mm, respectively. And, the height of billet is 120 mm. The mandrel diameter is 307.5 mm. The diameter and fillet radius of rollers are 116 and 10 mm, respectively. During spinning, the workpiece was tied with mandrel and rotates together, while three rollers fed along the axial direction at the same time. The tube blank was set as a deformable body and discretized by element meshing. As for the thermal events, mandrel and roller were assumed to be isothermal. In addition, conversion rate from

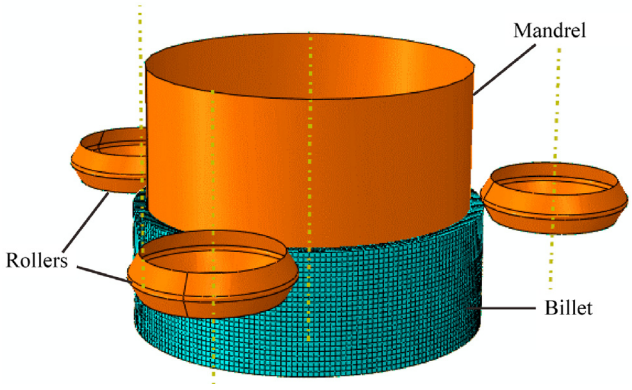

Fig. 1 FE model of hot spinning of titanium alloy thin-walled tube.

Table 1 Hot spinning processing parameters.

Parameters	Value
Attack angle (°)	22.5
Mandrel rotation speed (rad/s)	9.32
Roller feed rate (mm/r)	1
Wall thickness reduction	50%
Initial mandrel temperature (℃)	350
Initial spinning temperature (℃)	800

deformation energy to thermal energy was set as 0.9. Coulomb's friction model was applied to describe the friction between workpiece and tools. And, the friction coefficient was 0.1. The detailed processing parameters in hot spinning are shown in Table 1.

During the FE modelling, to simulate the effects of microstructure and stress state on fracture behaviour, a hybrid constitutive model was applied to describe the material deformation behaviour. This constitutive model was developed in previous work [21], which can predict the microstructure evolution, damage and fracture, and flow stress simultaneously. Moreover, the dependence of damage on microstructure evolution and stress state was considered. This constitutive model mainly consists of two modules: microstructure model and damage model. The microstructure model is a physically-based intrinsic state variable model, which considers the phase transformation and DRX during hot deformation. Their key formulations are Eqs. (1) and (2), respectively.

$$\begin{cases} f_\alpha = \zeta_1\{1-\exp[\zeta_2(\zeta_3 - T)]\} \\ f_\beta = 1 - f_\alpha \end{cases} \tag{1}$$

where f_α is α phase fraction, f_β is β phase fraction, T is temperature. ζ_1, ζ_2 and ζ_3 are material constant.

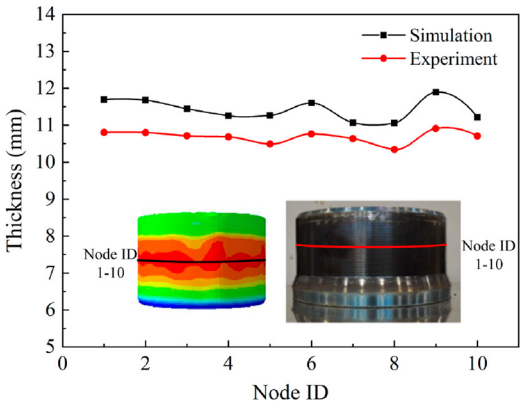

(a) Thickness distribution

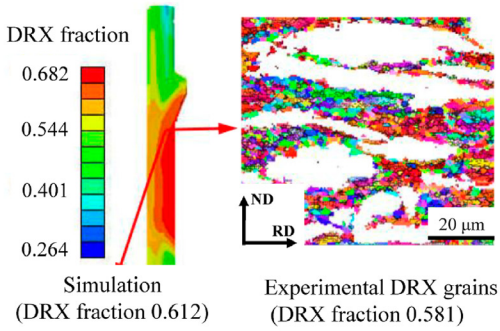

(b) DRX fraction

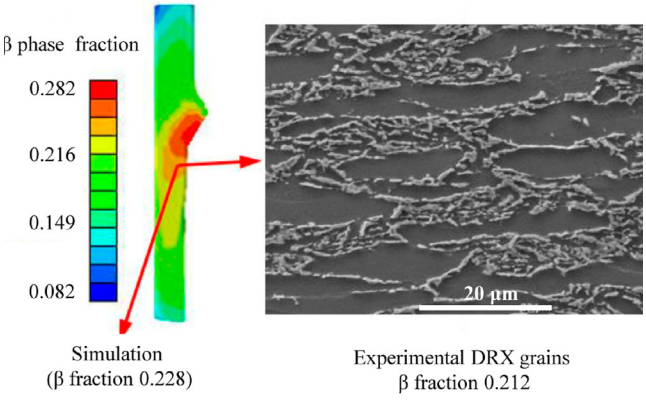

(c) β phase fraction

Fig. 2 Forming results obtained by simulation and experiment.[21]

$$\dot{S} = c_0(1-S)\left(\dot{\varepsilon}_{\mathrm{m}}^{\mathrm{p}}\right)^{c_1}\theta(\varepsilon_{\mathrm{p}} - \varepsilon_{\mathrm{c}})M_{\mathrm{b}}P/d \tag{2}$$

where S means the DRX fraction, c_0 and c_1 are material constant, θ is step function. ε_{p} is plastic strain, $\dot{\varepsilon}_{\mathrm{m}}^{\mathrm{p}}$ is the plastic strain rate in matrix. ε_{c} is the critical strain producing DRX.

Table 2 Chemical composition of TA15 alloy.

Element	Ti	Al	Mo	Zr	V	Fe	Impurity
Content (wt%)	Matrix	6.1–6.5	0.9–1.2	1.9–2.2	0.8–1.3	0.25	<0.3

Table 3 Quantitative comparisons between simulation and experiment results.

Type	Predicted result	Experimental result	Relative value (%)
Wall thickness			13.2 (maximum)
DRX fraction	0.612	0.581	5.3
β phase fraction	0.228	0.212	7.5

M_b, d and P are grain-boundary mobility, grain diameter and driving force per unit area, respectively. The damage model is developed by introducing DRX fraction, β phase fraction and stress triaxiality into Gurson-Tvergaard-Needleman model. The detail modifications are focused on the representations of void nucleation strain ε_N, void growth factor χ, critical condition for void coalescence f_c and the shear effect on void growth df_s, as the following four equations, respectively.

$$\varepsilon_N = \varepsilon_{N_0}\left[\exp\left(C_s S + C_\beta f_\beta^*\right)\right] \tag{3}$$

$$\chi = \chi_0\left[\exp\left(D_s S + D_\beta f_\beta^*\right)\right] \tag{4}$$

$$f_c = f_{c_0}\left[\exp\left(E_s S + E_\beta f_\beta^*\right)\right] \tag{5}$$

$$\mathrm{d}f_s = k_w w f \frac{s_{ij}\mathrm{d}\varepsilon_{ij}^{\mathrm{p}}}{\bar{\sigma}} \tag{6}$$

in Eqs. (3)–(5), ε_{N_0}, χ_0, f_{c_0} are reference values. f_β^* is related to β phase fraction. C_s, D_s, E_s and C_β, D_β, E_β are coefficients related with DRX fraction and β phase fraction. In Eq. (6), k_w is the damage growth rate under pure shear, S_{ij} and $\mathrm{d}\varepsilon_{ij}^{\mathrm{p}}$ represent the deviatoric stress tensor and strain increment, w and f describe the stress state and the current void volume fraction, respectively. These adaptations make it be able to simulate the effects of microstructure evolution and stress state on the damage and fracture. The above Eqs. (1)–(6) are just some key formulations of the constitutive model, whose detailed description of model and parameters can be referred to.[21] When integrating the constitutive model into FE model, the damage accumulation just occurs when the material experiences tensile plastic strain under the tensile hydrostatic stress state. While, no damage evolution occurs when the material undergoes plastic strain under compressive hydrostatic stress state due to the crack closure effect.[22] Besides, the critical void volume fraction (VVF) for producing fracture is calibrated as 0.15 in previous work,[21] which is the key criterion for judging the fracture defect.

The FE model was verified by the hot spinning experiment, whose processing conditions are the same to those listed in Table 1. In experiment, an annealed two-phase TA15 (Ti-6Al-2Zr-1Mo-1 V) alloy was used. Its chemical composition is listed in Table 2. The initial microstructure consists of 60% α phase and residual β transformation matrix. The transformation temperature of α/β phase is 1263 K. Meanwhile, the average grain size is 20 μm. The hot spinning experiment was conducted on HO-018 CNC horizontal spinning machine of Xi'an Aerospace Power Machinery Factory. The spinning machine has three rollers and is equipped with a flame gun to heat the workpiece and mandrel during forming, which is suitable for the hot spinning processing of straight tube.

A specific location at the center of the cross section of spun tube were selected to compare microstructure quantitatively in simulation and experiment. The size of this location is about 100 μm × 100 μm. In experiment, the microstructure was observed by scanning electron microscope (SEM) using TESCAN VEGA. Meanwhile, electron back-scattered diffraction (EBSD) was conducted on the samples to obtain characteristics of DRX grains using Zeiss Merlin Compact. Before EBSD, the samples were electro-polished with a solution (5% $HClO_4$ + 30% CH_3OH + 65% $C_4H_{10}O$). After EBSD, the microstructure characteristics were quantitatively analyzed through the HKL-Channel 5 software. In addition, along the circumferential direction of the formed tube, 10 nodes were selected equidistantly at the middle of the height. Then the thickness at these nodes of simulation and experiment were measured separately. Fig. 2 shows the thickness distribution, DRX fraction and β phase fraction obtained by simulation and experiment. Their quantitative values and relative errors are given in Table 3. It can be found that the thickness distribution in simulation and experiment are very close, presenting the maximum error of 13.2%. On the other hand, the simulated DRX fraction and β phase fraction in formed region also agree well with the experimental result. These indicate that the FE model can simulate both of the macro-deformation and

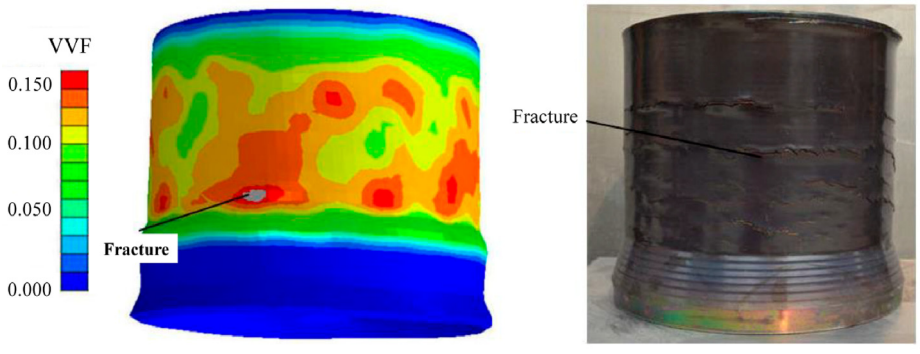

(a) Simulation with thickness reduction of 68.9% (b) Experiment with thickness reduction of 71.2%

Fig. 3 Fracture defect in FE simulation and experiment.

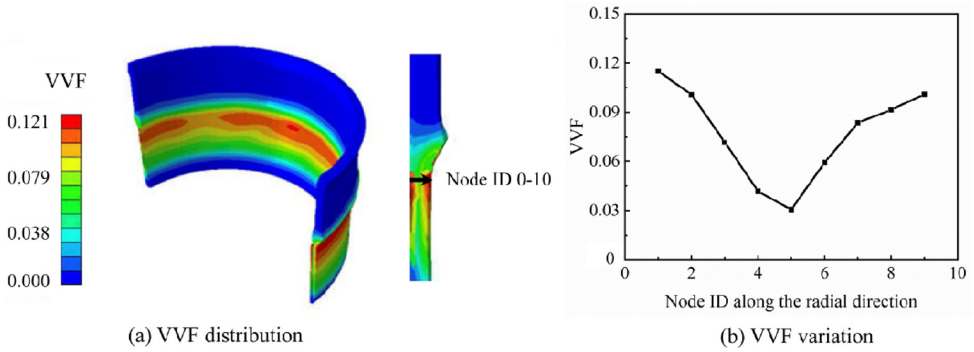

(a) VVF distribution (b) VVF variation

Fig. 4 Distribution of VVF in spun tube and variation with tracked nodes along radial direction in deformed area.

microstructure evolution accurately. In addition, a set of spinnability experiments were conducted to verify the prediction accuracy of damage and fracture. As shown in Fig. 3, the fracture defect was produced when the thickness reduction increases to 68.9% in FE simulation, and the fracture defect occurs when the thickness reduction increases to 71.2% in experiment. The simulation and experiment results agree very well. The above comparisons suggest that the FE model is valid and can be applied for predicting the macro-shape, microstructure evolution, damage and fracture phenomena during hot spinning of TA15 alloy tube.

3. Results and discussion

3.1. Characteristics of damage and fracture defect

Ductile fracture of material is a result of damage accumulation through the void nucleation, growth and coalescence. The fracture defect occurs when the VVF reaches a critical value, thus, VVF is an important index evaluating the damage degree. Larger VVF means greater damage degree and the fracture is easier to occur. So, the distribution of VVF on workpiece was employed to analyze the characteristics of damage and fracture in hot spinning in this section.

Fig. 4 shows the distribution of VVF in the spun tube and variation of VVF with tracked nodes (black arrow in Fig. 4 (a)) along the radial direction in the deformed area. It can be seen that the VVF is unevenly distributed along the radial direction. It presents larger value on the outer and inner surfaces, while smaller value in the middle-thickness region. In addition, the largest VVF occurs at the inner surface (Fig. 4 (b)), which indicates that the fracture is most likely to occur at the inner surface during hot spinning. These results are caused by the combined effects of stress state, strain state and microstructure evolution of material during forming process. Generally, positive stress triaxiality and tensile plastic strain will promote the nucleation, growth and coalescence of voids.[23] The tensile plastic strain refers to the plastic strain under tensile hydrostatic stress, which have a great effect on the evolution of micro voids.[22] As for microstructure evolution, $\alpha \leftrightarrow \beta$ phase transformation and DRX are two main factors affecting the damage behavior in deformation of titanium alloy at high temperature. Larger DRX fraction and β phase fraction would restrain the damage evolution to some degree.[21] Thus, the distributions of stress triaxiality, tensile plastic strain, DRX fraction and β phase fraction during hot spinning were analyzed to explain the distribution features of VVF below.

Fig. 5 shows the distributions of stress triaxiality and tensile plastic strain in hot spinning. From Fig. 5 (a) and (c), it can be seen that the stress triaxiality are positive at the inner and

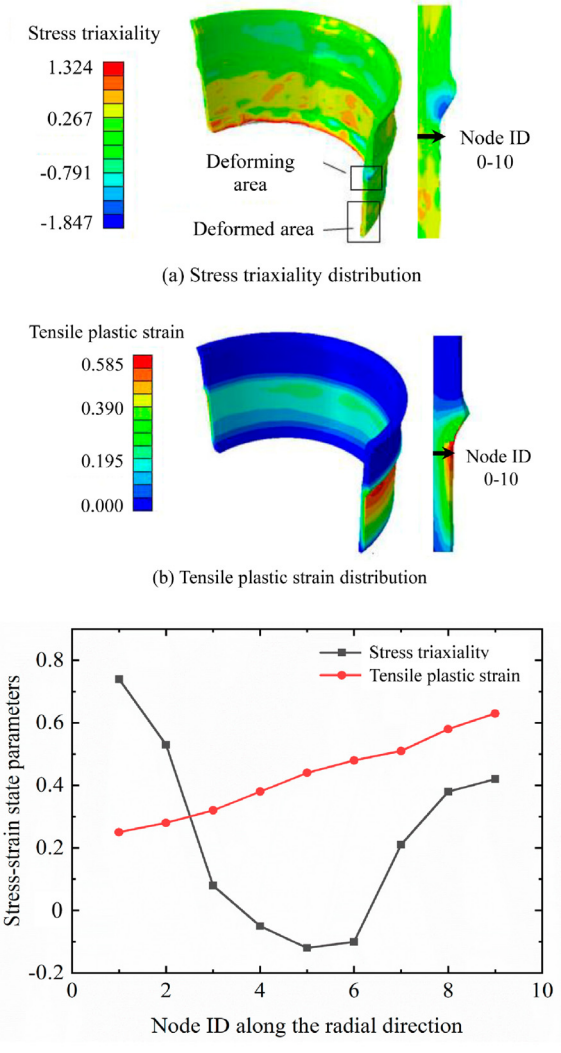

(a) Stress triaxiality distribution

(b) Tensile plastic strain distribution

(c) Variations with tracked nodes along the radial direction

Fig. 5 Distributions and variations of stress triaxiality and tensile plastic strain in spinning process.

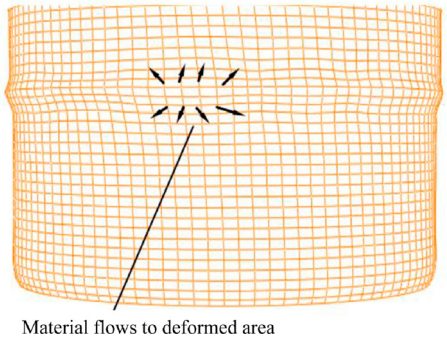

Fig. 6 Schematic of material flow in spinning process.

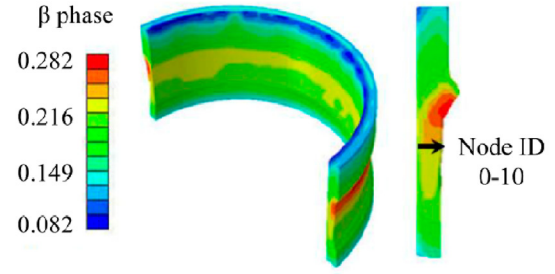

(a) β phase fraction distribution

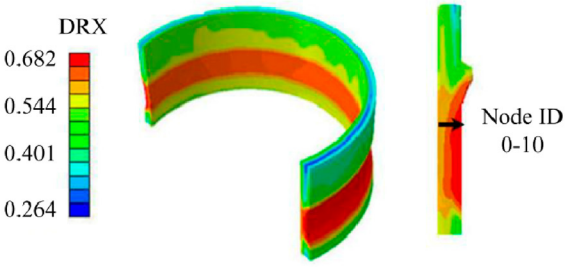

(b) DRX fraction distribution

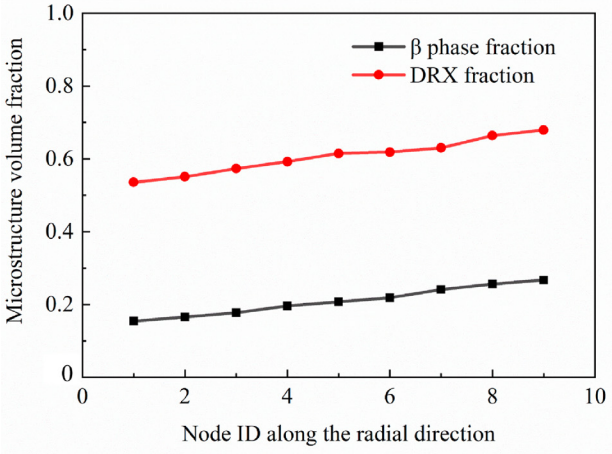

(c) Variations with tracked nodes along the radial direction

Fig. 7 Distributions and variations of microstructure in spinning process.

outer surfaces, while negative at the middle-thickness region. Another hand, it is found from Fig. 5 (b) and (c) that large tensile plastic strain exists in the spinning, and which increases from the inner surface to outer surface. This is related to the material flow in spinning, as shown in Fig. 6. Under the action of rollers, material will flow from the deforming area to the deformed area, thus producing the tensile plastic strain. Due to the direct action of rollers, the outer surface presents the largest tensile plastic strain.

The distributions of DRX fraction and β phase fraction in hot spinning of TA15 alloy are shown in Fig. 7. As can be seen from Fig. 7 (a) and (c), the β phase fraction decreases monotonously from the outer surface to inner surface. This is related to the uneven temperature distribution along the radial direction during hot spinning. The outer surface usually presents the highest temperature due to massive deformation heat produced under severe rolling deformation, thus producing more β phase fraction. On the contrary, the inner surface presents the lowest temperature because of significant heat transfer to the colder mandrel, thus leading to a smaller β phase fraction. From Fig. 7 (b) and (c), it can be seen that DRX fraction presents the same increase trend from the inner surface to outer surface. The higher temperature at the outer surface is helpful to improve the DRX fraction. Meanwhile, larger shear stress and strain at the outer surface also contribute to the uneven distribution of DRX fraction. This is because the shear stress and strain could change the DRX from discontinuous DRX dominated mechanism to continuous DRX dominated mechanism, and promote the DRX kinetics obviously.[24] As a result, the DRX fraction presents the largest value at the outer surface and the smallest value at the inner surface.

Synthesize the above distributions of stress triaxiality, tensile plastic strain, DRX fraction and β phase fraction, the distribution characteristic of VVF could be explained as follows. The largest VVF at inner surface is attributed to the superposition effects of positive stress triaxiality and the smallest DRX fraction and β phase fraction. On the contrary, the smallest VVF in middle-thickness region is a combined result of negative stress triaxiality and larger DRX fraction and β phase fraction. As for the VVF at outer surface, although its DRX fraction and β phase fraction are both the largest, the acceleration role on damage development by positive stress triaxiality and the largest tensile plastic strain is more significant. This leads to larger VVF at the outer surface, while, which is smaller than that at the inner surface.

3.2. Effects of processing parameters on damage and fracture behaviors

As analyzed above, the damage distribution is greatly related to three factors, i.e., the stress state, tensile plastic strain and microstructure evolution of material, in hot spinning. These three factors are significantly dependent on the processing parameters of spinning. In this section, effects of processing parameters on the damage distribution were analyzed and explained from the variations of above three factors. This is helpful to suppress the fracture defect by controlling the processing parameters.

The effects of processing parameters on damage were studied through FE simulation combing single factorial experiments. Four processing parameters were considered in this work, i.e., initial spinning temperature, spinning pass, roller feed rate and roller fillet radius. Table 4 shows the variable values, where the bolded value of each parameter is the default

Table 4 Parameter values in single factorial experiments.

Type	Value 1	Value 2	Value 3	Value 4	Value 5
Initial spinning temperature (℃)	700	750	**800**	850	
Spinning pass	**1**	2	3	4	5
Roller feed rate (mm/s)	0.5	**1**	1.5	2	3
Roller fillet radius (mm)	5	**10**	15	20	25

value adopted when investigating the effect of other parameters on damage.

3.2.1. *Effect of initial spinning temperature*

Fig. 8 shows the variation of damage distribution along the radial direction with initial spinning temperatures. It can be seen that the VVF decreases monotonously with the temperature increasing. Fig. 9 shows the variations of DRX fraction, β phase fraction, stress triaxiality and tensile plastic strain along the radial direction at different temperatures. From Fig. 9 (a), it can be seen that the DRX fraction and β phase fraction both increase monotonously with temperature, which is because that higher temperature can promote the DRX kinetics and $\alpha \leftrightarrow \beta$ phase transformation during hot working of titanium alloy. These variations of microstructure evolution are helpful to suppress the void evolution and decrease the VVF to a great extent. In addition, it can be seen from Fig. 9 (b) and (c) that the stress triaxiality and tensile plastic strain remain nearly unchanged with temperature. These results suggest that the decrease of VVF with temperature increasing is mainly attributed to the microstructure effect, i.e., the increase of DRX fraction and β phase fraction.

3.2.2. *Effect of spinning pass*

Fig. 10 shows the final damage distributions along the radial direction in the deformed area after different spinning passes. It is noted that the total thickness reductions of five processing schemes are all 50%. As can be seen that with the increase of spinning pass, VVF decreases first and then increases with a critical value of 4 passes. Fig. 11 displays the variations of DRX fraction, β phase fraction, stress triaxiality and tensile plastic strain with spinning passes. It can be seen from

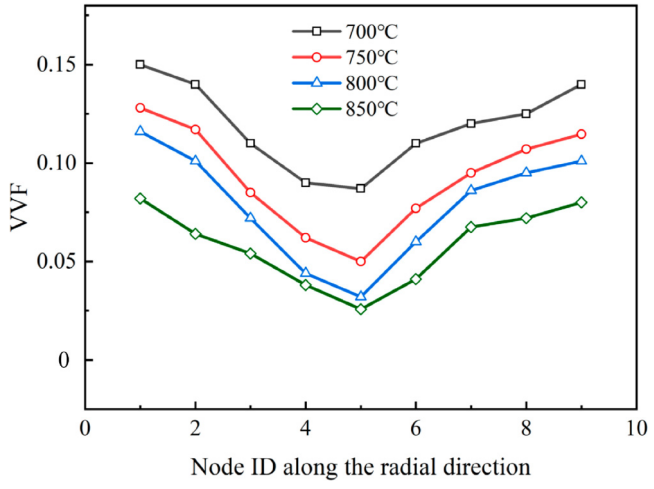

Fig. 8 Variation of VVF distribution along radial direction with initial spinning temperatures.

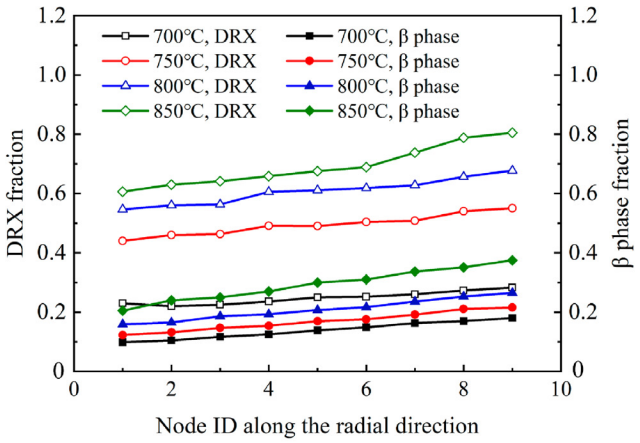

(a) Microstructure

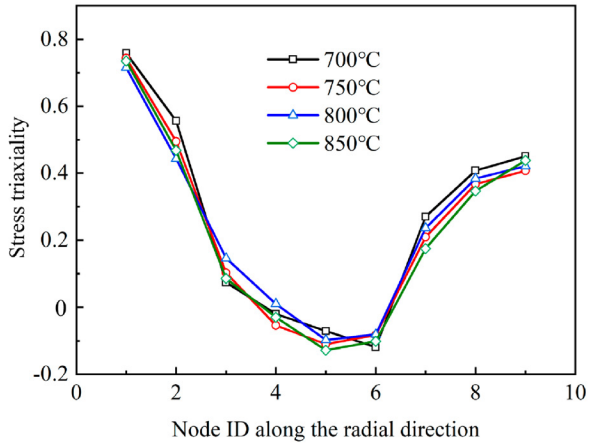

(b) Stress triaxiality

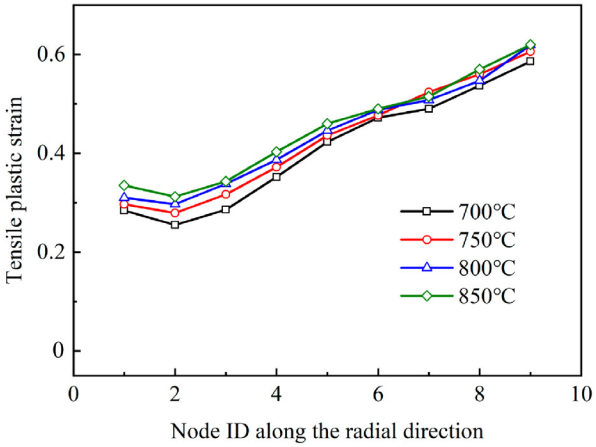

(c) Tensile plastic strain

Fig. 9 Variations of distributions of microstructure, stress triaxiality and tensile plastic strain with initial spinning temperatures.

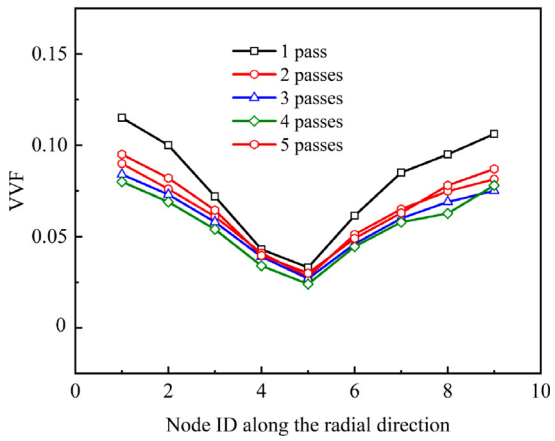

Fig. 10 Variation of VVF distribution along radial direction with spinning pass.

Fig. 11 (a) that the DRX fraction and β phase fraction both decrease monotonously with the spinning pass increasing. These are caused by the decrease of workpiece temperature due to more heat exchange and loss to surrounding environment under more spinning passes. Lower temperature suppresses the α → β phase transformation and DRX kinetics, then results in the decrease of DRX fraction and β phase fraction. This would accelerate the void accumulation and increase the VVF. On the other hand, it is found from Fig. 11(b) that the stress triaxiality decreases with spinning pass increasing. This is because the decrease of thickness reduction in each spinning pass makes less material to deform in the front of rollers, which will further decrease the stress triaxiality.[25] Thus, considering the decrease of stress triaxiality, the damage evolution and VVF will be suppressed with the spinning pass increasing. As for the tensile plastic strain, it varies little with the spinning pass, as shown in Fig. 11 (c). Based on the above analysis, it can be concluded that the early decrease of VVF with increasing spinning pass is mainly attributed to the reduction of stress triaxiality. While, the later increase of VVF with spinning pass mainly depends on the decrease of DRX fraction and β phase fraction. In other words, the variation of VVF with the spinning pass is dominated by the stress state at smaller spinning pass, but dominated by the microstructure evolution at larger spinning pass.

3.2.3. Effect of roller feed rate

Fig. 12 displays the variation of damage distribution along the radial direction with feed rate. It can be seen that the VVF decreases first and reaches the smallest value at 1.5 mm/r, then increases with the feed rate increasing. Fig. 13 shows the distributions of DRX fraction, β phase fraction, stress triaxiality and tensile plastic strain under different feed rates. The DRX fraction and β phase fraction both gradually increase with feed rate, as shown in Fig. 13 (a). These are mainly related to the variation of workpiece temperature with feed rate. As the feed rate increases, the forming time becomes shorter and less heat is dissipated from the workpiece. Thus, the workpiece temperature increases with feed rate, which promotes α → β phase transformation and DRX kinetics. From Fig. 13 (b), it can be seen that the stress triaxiality also increases monotonously with feed rate. This is mainly caused by more material accumulating in the front of rollers with feed rate increasing. On the contrary, the tensile plastic strain is decreased monotonously with feed rate increasing, as shown in Fig. 13 (c). This is because helical angle of roller trajectory increases with roller feed rate, which will make less material rolled by rollers, as shown in Fig. 14. It will then decrease the tensile plastic strain. The above analyses suggest that the early decrease of VVF

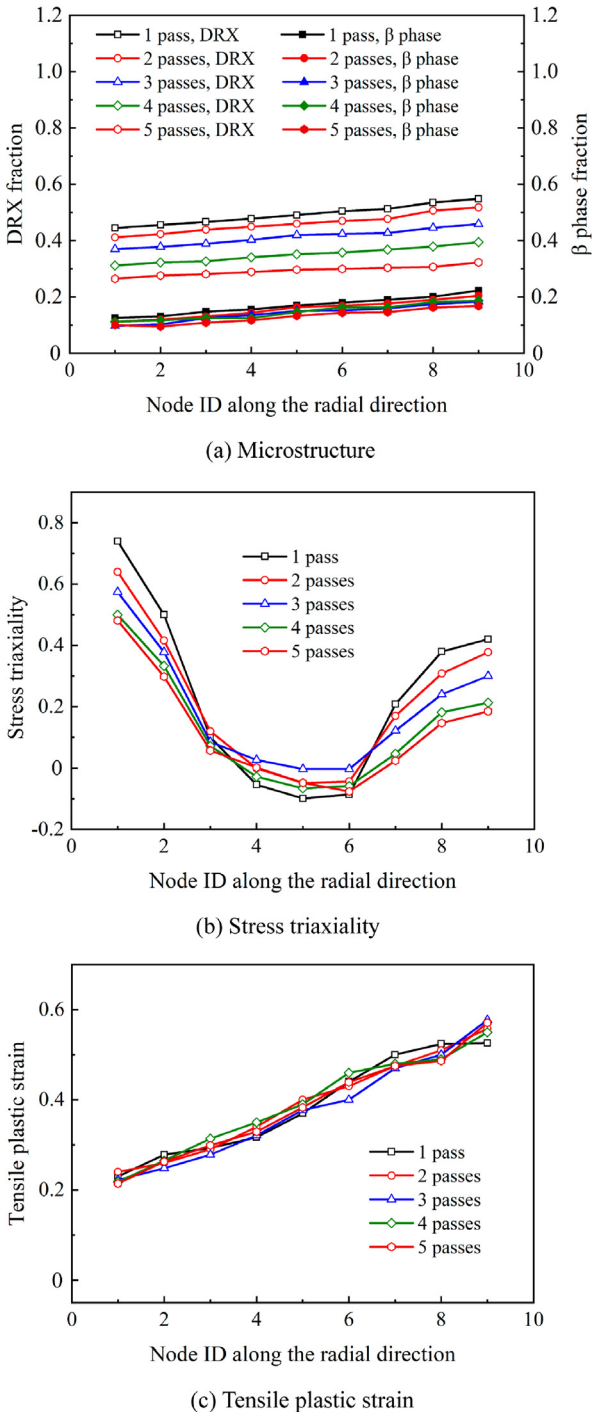

Fig. 11 Variations of distributions of microstructure, stress triaxiality and tensile plastic strain with spinning pass.

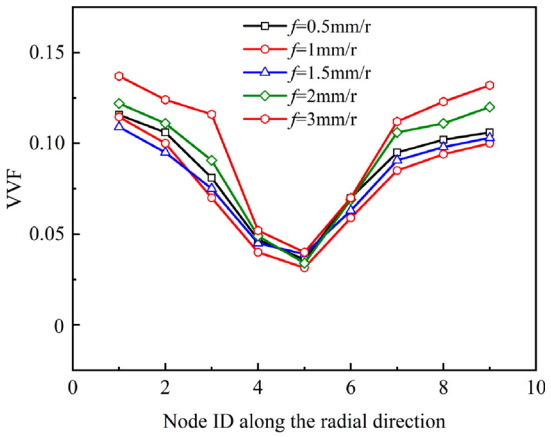

Fig. 12 Variation of VVF distribution along radial direction with feed rate.

with increasing feed rate is mainly caused by the reduction of tensile plastic strain and the increases of DRX fraction and β phase fraction. However, the later increase of VVF with feed rate mainly depends on the increase of stress triaxiality. That is to say, the variation of VVF with feed rate is dominated by tensile plastic strain and microstructure at smaller feed rate, while mainly controlled by stress triaxiality at larger feed rate.

3.2.4. Effect of roller fillet radius

The variations of damage distribution along radial direction with the roller fillet radius are given in Fig. 15. It can be seen that the VVF gradually decreases with the increase of roller fillet radius. Fig. 16 shows the distributions of β phase fraction, DRX fraction, stress triaxiality and tensile plastic strain under different roller fillet radii. From Fig. 16 (a) and (b), it is found that the DRX fraction, β phase fraction and stress triaxiality all change little with the roller fillet radius. On the other hand, the tensile plastic strain gradually decreases with the increase of roller fillet radius, as shown in Fig. 16 (c). This is because the contact area between the workpiece and rollers increases with the roller fillet radius increasing, as given in Fig. 17. This will reduce the flow resistance of material from the deforming area to the deformed area, thus decreasing the tensile plastic strain. Therefore, the damage evolution and VVF were suppressed with the increase of roller fillet radius. And, it can be inferred that the variation of damage with roller fillet radius is mainly determined by the tensile plastic strain, while irrelevant with the microstructure and stress triaxiality.

According to the above analyses in Sections 3.2.1–3.2.4, the variations of VVF with processing parameters and the underlying dominant influencing mechanisms were summarized in Table 5. The symbol ↑ and ↓ represent the positive and negative correlation between VVF and processing parameter, respectively.

3.3. Improvement of forming limit by controlling damage and fracture

As analyzed in Section 3.2, the processing parameters significantly affect the damage and fracture behavior, which will further determine the forming limit. i.e., the maximum thickness reduction without fracture defect, in hot spinning of TA15

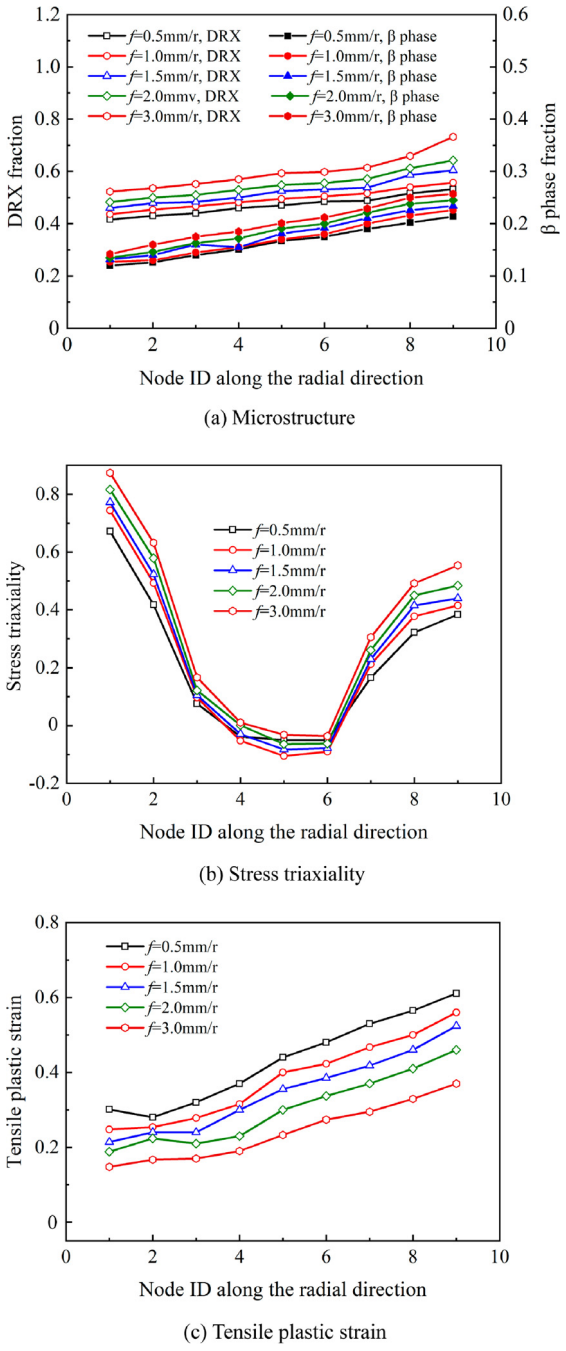

Fig. 13 Variations of distributions of microstructure, stress triaxiality and tensile plastic strain with roller feed rate.

alloy tube. In this section, the dependence of forming limit on processing parameters were obtained first, based on which the processing parameters were optimized to improve the forming limit.

The variation of forming limit with processing parameters was also analyzed through the single factorial experiments in Section 3.2. For a certain processing condition, the forming limit is determined by stepwise searching method. During stepwise searching, the initial thickness reduction and step size are set as 50% and 5%, respectively. In any searching step, if no fracture occurs, plus the step size to current thickness reduc-

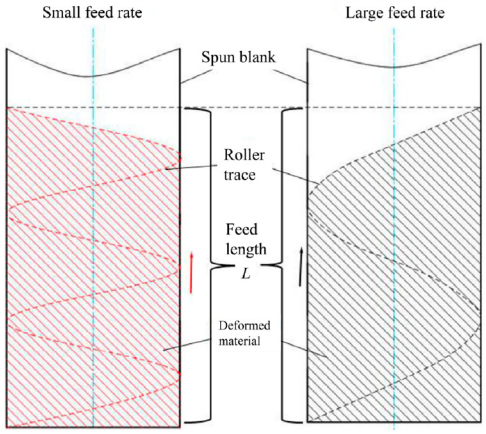

Fig. 14 Schematic of material compressed by rollers under different roller feed rates.

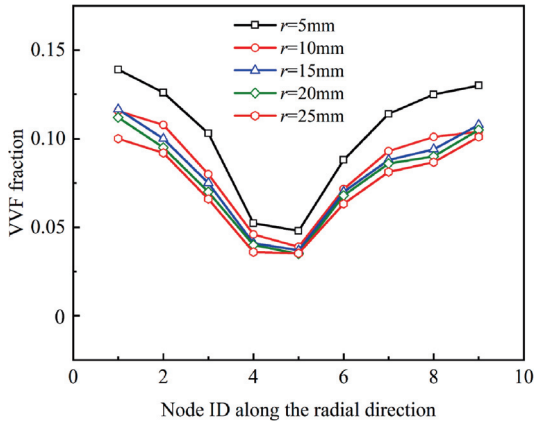

Fig. 15 Variation of VVF distribution along radial direction with roller fillet radius.

tion and go to the next step; if the fracture appears, halve the step size and try again. Repeat the above searching step until the forming limit is determined. Fig. 18 shows the variation of forming limit with processing parameters. It can be seen that the forming limit increases monotonously with temperature. While, it increases first and then decreases with the increases of spinning pass and roller feed rate. In addition, it reaches the greatest value under 4 passes and 1.5 mm/r, respectively. With the roller fillet radius increasing, the forming limit increases gradually and the increasing trend is more significant when the radius is small.

Based on the results shown in Fig. 18, an optimal combination of processing parameters can be determined to achieve a higher forming limit as follows: spinning initial temperature 850 °C, spinning pass 4, roller feed rate 1.5 mm/r, roller fillet radius 25 mm. By the combination of FE simulation and step-

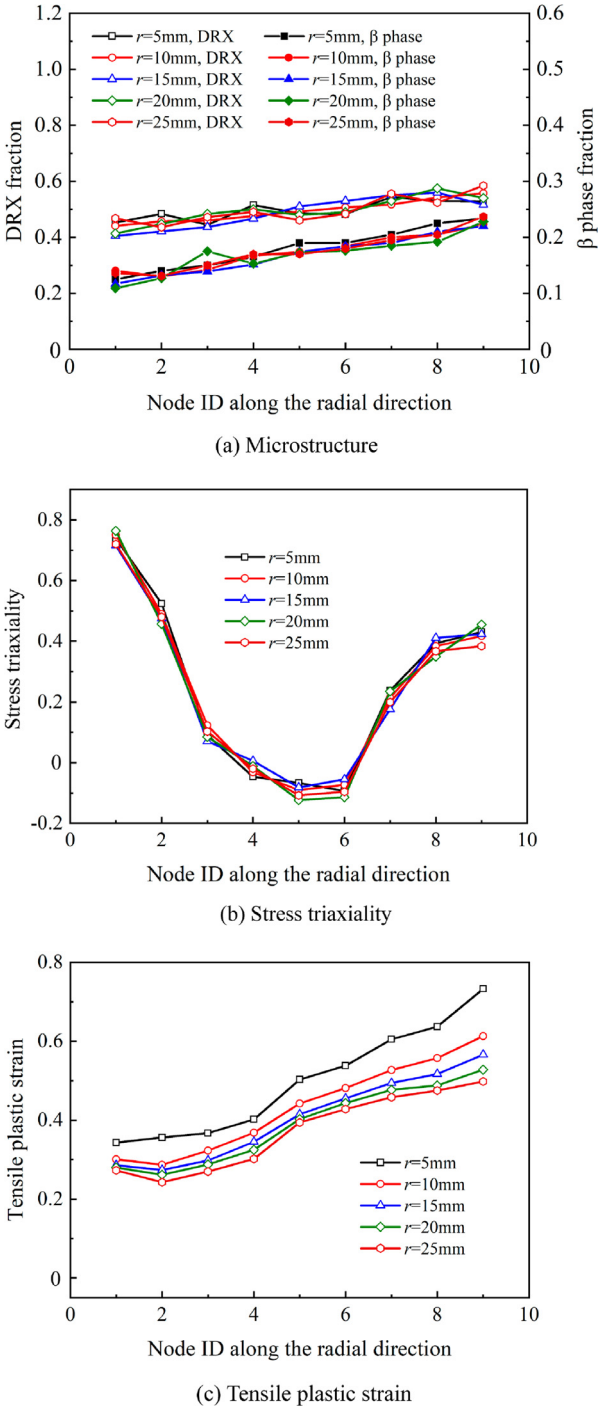

Fig. 16 Variations of distributions of microstructure, stress triaxiality and tensile plastic strain with roller fillet radius.

wise searching method, the forming limit under the optimal processing condition was determined as 86.7%. The simulated result with 86.7% reduction is shown in Fig. 19 (a). Moreover,

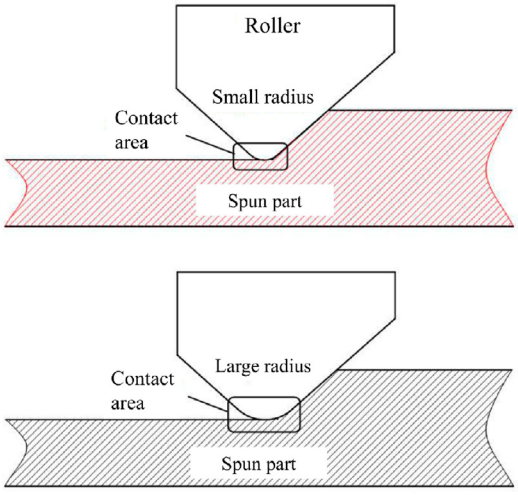

Fig. 17 Schematic of contact area between roller and spun part under different roller fillet radii.

Table 5 Summary of variation law of VVF with processing parameter and underlying dominate influencing mechanisms.

Processing parameters	Variation of VVF	Dominate influencing mechanism
Initial spinning temperature	↑	Microstructure
Spinning pass	↓ (≤4), ↑ (>4)	Stress triaxiality (Early), Microstructure (Later)
Roller feed rate (mm/r)	↓ (≤1.5), ↑ (>1.5)	Tensile plastic strain and Microstructure (Early), Stress triaxiality (Later)
Roller fillet radius	↓	Tensile plastic strain

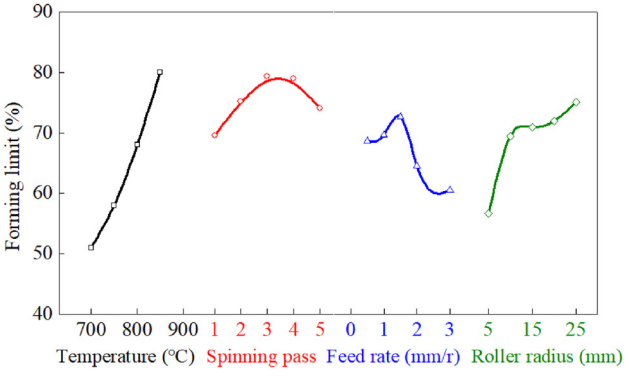

Fig. 18 Variations of forming limit with processing parameters in hot spinning of TA15 alloy tube.

the corresponding hot spinning experiment was conducted to verify the result, as shown in Fig. 19 (b). It can be seen that no fracture defect occurs, which suggests that the optimized parameters can achieve effective control of ductile fracture and improve the forming limit significantly.

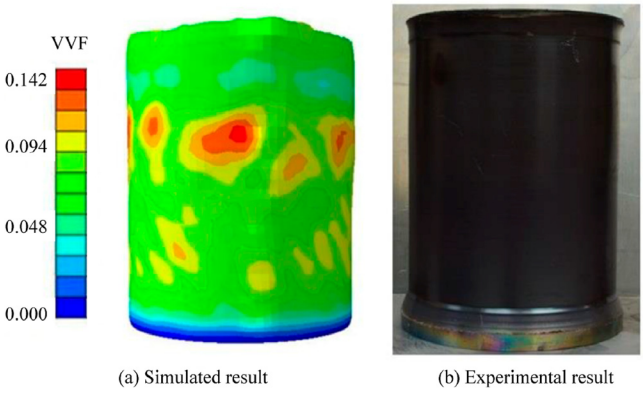

Fig. 19 Simulated and experimental results of hot spun part with a thickness reduction of 86.7% under optimized processing parameters.

4. Conclusions

In this research, the dependences of damage and fracture on processing parameters in hot spinning of thin-walled TA15 alloy tube were investigated by simulation based on an integrated FE model considering microstructure and damage evolution and physical experiment. The formability of TA15 alloy tube in hot spinning process was improved by optimizing the processing parameters to control the fracture defect. The main conclusions are as follows:

(1) For the damage distribution on workpiece, the inner surface presents the largest void volume fraction (VVF) and greatest risk of fracture, which is mainly attributed to the superposition effects of positive stress triaxiality and the smallest DRX fraction and β phase fraction at inner surface. On the contrary, the middle-thickness region presents the smallest VVF, where there exists a combined effect negative stress triaxiality and larger DRX fraction and β phase fraction.

(2) With the increase of the initial spinning temperature, VVF is gradually decreased due to the increases of DRX fraction and β phase fraction. With the increase of spinning pass, the VVF is firstly decreased and then increased. The early decrease is mainly attributed to the decrease of stress triaxiality; while the later increase is mainly depended on the decrease of DRX fraction and β phase fraction. Similarly, the VVF is decreased first and then increased with the increasing roller feed rate. The early decrease is mainly caused by the reduction of tensile plastic strain and the increases of DRX fraction and β phase fraction, the later increase, however, is mainly depended on the increase of stress triaxiality. On the other hand, the VVF is decreased monotonously with roller fillet radius because of the decrease of tensile plastic strain.

(3) By the combination of FE simulation and stepwise searching method, the forming limit, i.e., the maximum thickness reduction without fracture defect, was determined under different processing conditions. Moreover, an optimal configuration of processing parameters was proposed to improve the forming limit of thin-walled

TA15 alloy tube in hot spinning: spinning initial temperature 850 °C, spinning pass 4, feed rate 1.5 mm/r, roller fillet radius 25 mm. Under these optimal parameters, the forming limit was improved to 86.7%.

Declaration of Competing Interest

The authors declare that they have no known competing financial interests or personal relationships that could have appeared to influence the work reported in this paper.

Acknowledgments

The authors would acknowledge the funding support from the National Natural Science Foundation of China (No. 51875467, 92060107), National Science Fund for Distinguished Young Scholars of China (No. 51625505), the Hong Kong Scholar Program (No. XJ2018010), the Young Elite Scientists Sponsorship Program by CAST (No. 2018QNRC001) and the Research Fund of the State Key Laboratory of Solidification Processing (NPU), China (Grant No. 2019-TS-10).

References

1. Lütjering G, Williams JC. *Titanium*. 2nd ed. Berlin Heidelberg: Springer-Verlag; 2007.
2. Ning Y, Fu MW, Hou H, Yao Z, Guo H. Hot deformation behavior of Ti-5.0Al-2.40Sn-2.02Zr-3.86Mo-3.91Cr alloy with an initial lamellar microstructure in the α + β phase field. *Mater Sci Eng, A* 2011;**528**(3):1812–8.
3. Yang Q, Cheng C, El-Aty AA, et al. Effects of punch size, magnetic field, and magnetorheological elastomers medium on forming T-shaped thin-walled Inconel 718 tubes. *Chinese J Aeronaut* 2020. https://doi.org/10.1016/j.cja.2020.09.032.
4. Wong CC, Dean TA, Lin J. A review of spinning, shear forming and flow forming processes. *Int J Mach Tool Manuf* 2003;**43**(14):1419–35.
5. Xu WC, Shan DB, Yang GP, et al. Hot spinning of cylindrical workpieces of TA15 titanium alloy. *Rare Met* 2007;**26**:255–61.
6. Wang Y, Su H, Qian N, et al. Neck-spinning quality analysis and optimization of process parameters for plunger components: Simulation and experimental study. *Chinese J Aeronaut* 2021;**34**(4):174–91. https://doi.org/10.1016/j.cja.2020.08.040.
7. Lin YC, Qian S-S, Chen X-M, Li X-H, Yang H. Staggered spinning of thin-walled Hastelloy C-276 cylindrical parts: Numerical simulation and experimental investigation. *Thin-Walled Struct* 2019;**140**:466–76.
8. Zhan M, Gu C, Jiang Z, Hu L, Yang He. Application of ductile fracture criteria in spin-forming and tube-bending processes. *Comp Mater Sci* 2009;**47**(2):353–65.
9. Zhan M, Guo J, Fu MW, et al. Formability limits and process window based on fracture analysis of 5A02-O aluminum alloy in splitting spinning. *J Mater Process Tech* 2018;**257**:15–32.
10. Zeng R, Ma F, Huang L, Li J. Investigation on spinnability of profiled power spinning of aluminum alloy. *Int J Adv Manuf Technol* 2015;**80**(1-4):535–48.
11. Ma H, Xu W, Jin BC, Shan D, Nutt SR. Damage evaluation in tube spinnability test with ductile fracture criteria. *Int J Mech Sci* 2015;**100**:99–111.
12. Xu W, Wu He, Ma H, Shan D. Damage evolution and ductile fracture prediction during tube spinning of titanium alloy. *Int J Mech Sci* 2018;**135**:226–39.
13. Zhan M, Zhang T, Yang He, Li L. Establishment of a thermal damage model for Ti-6Al-2Zr-1Mo-1V titanium alloy and its application in the tube rolling-spinning process. *Int J Adv Manuf Technol* 2016;**87**(5-8):1345–57.
14. Gao P, Fu M, Zhan M, Lei Z, Li Y. Deformation behavior and microstructure evolution of titanium alloys with lamellar microstructure in hot working process: A review. *J Mater Sci Technol* 2020;**39**:56–73.
15. Lin YC, Pang G-D, Jiang Y-Q, et al. Hot compressive deformation behavior and microstructure evolution of a Ti-55511 alloy with basket-weave microstructures. *Vacuum* 2019;**169**:108878. https://doi.org/10.1016/j.vacuum.2019.108878.
16. OuYang DL, Fu MW, Lu SQ. Study on the dynamic recrystallization behavior of Ti-alloy Ti-10V-2Fe-3V in β processing via experiment and simulation. *Mater Sci Eng, A* 2014;**619**:26–34.
17. Shang X, Cui Z, Fu MW. A ductile fracture model considering stress state and Zener-Hollomon parameter for hot deformation of metallic materials. *Int J Mech Sci* 2018;**144**:800–12.
18. Shang XQ, Cui ZS, Fu MW. Dynamic recrystallization based ductile fracture modelling in hot working of metallic materials. *Int J Plast* 2017;**95**:105–22.
19. Ran JQ, Fu MW. A hybrid model for analysis of ductile fracture in micro-scaled plastic deformation of multiphase alloys. *Int J Plast* 2014;**61**:1–16.
20. Dong J, Wang S, Zhou J, Ma C, Wang S, Yang Bo. Experimental and numerical investigation on the shearing process of stainless steel thin-walled tubes in the spent fuel reprocessing. *Thin-Walled Struct* 2019;**145**:106407. https://doi.org/10.1016/j.tws.2019.106407.
21. Gao PF, Guo J, Zhan M, Lei ZN, Fu MW. Microstructure and damage based constitutive modelling of hot deformation of titanium alloys. *J Alloy Compd* 2020;**831**:154851. https://doi.org/10.1016/j.jallcom.2020.154851.
22. Bouchard P-O, Bourgeon L, Fayolle S, Mocellin K. An enhanced Lemaitre model formulation for materials processing damage computation. *Int J Mater Form* 2011;**4**(3):299–315.
23. Gao X, Zhang T, Zhou J, Graham SM, Hayden M, Roe C. On stress-state dependent plasticity modeling: Significance of the hydrostatic stress, the third invariant of stress deviator and the non-associated flow rule. *Int J Plast* 2011;**27**(2):217–31.
24. Wang XX, Zhan M, Gao PF, et al. Deformation mode dependent mechanism and kinetics of dynamic recrystallization in hot working of titanium alloy. *Mater Sci Eng, A* 2020;**772**:138804. https://doi.org/10.1016/j.msea.2019.138804.
25. Huang L, Yang He, Zhan M, Hu L. Forming characteristics of splitting spinning based on the behaviors of roller. *Comp Mater Sci* 2009;**45**(2):449–61.